Solid State Science and Technology, Vol. 19, No2 (2011) 249-258
ISSN 0128-7389

STRUCTURE AND MICROSTRUCTURE STUDY ON $LaMnO_3$ AND $La_{0.67}Ba_{0.33}MnO_3$: COMPARISON BETWEEN BULK AND THIN FILMS

J.K. Wong*, K.P. Lim, S.A. Halim, S.K. Chen,
S.W. Ng and H.M. Albert Gan

Superconductor and Thin Film Laboratory, Department of Physics, Faculty of Science, Universiti Putra Malaysia, 43400 UPM Serdang, Selangor, Malaysia.

**Corresponding author: wjenkuen@hotmail.com*

ABSTRACT

Bulk $LaMnO_3$ and $La_{0.67}Ba_{0.33}MnO_3$ polycrystalline manganite were prepared via solid-state reaction and converted into thin films via pulsed laser deposition technique. Comparison between bulk and thin films on structure and microstructure were studied. Crystal structure transformation was observed when bulk $LaMnO_3$ converted into thin film. Clear grains was observed in bulk $LaMnO_3$ while $LaMnO_3$ thin film shows melted-like grains accompanied by island growth mode. Positive misfit was observed in $La_{0.67}Ba_{0.33}MnO_3$ thin films due to strains induced by the lattice misfit between the deposited film and substrate. Nano-sized cracks were observed due to dissimilarity in coefficient of thermal expansion between thin film and substrate. In both $LaMnO_3$ and $La_{0.67}Ba_{0.33}MnO_3$ systems, larger lattice strain was observed in thin film sample compared to bulk. Thus, enhanced the density of system by invoke MnO_6 octahedral to stretch its Mn-O-Mn bond angle and Mn-O bond length. Denser crystal system was observed in thin film sample compared to bulk.

Keywords: Crystal structure; Lattice strain; Manganites; Microstructure and Thin film;

INTRODUCTION

The discovery of Colossal Magnetoresistance (CMR) from $LnMnO_3$ (Ln= rare earth element) manganite perovskite with general formula of $Ln_{1-X}A_XMnO_3$ (A= divalent alkaline earth cation) had stimulated many interest not only for the fundamental sciences but also their potential application in magnetic sensor industries [1-2]. In conventional application, most of these materials often prepared in the form of thin films, multilayer or hybrid systems to improve materials usage efficiency reduce costs and provide performance not possible with bulk materials. However, the properties of manganite thin films are different especially its electrical transport and magnetoresistive behavior as compared to bulk. It was found that the lattice strain due to the epitaxial growth of the film plays an important role in formation of the spin and charge ordered state which will affect the CMR effect [3-6]. Since the conducting mechanism are governed by Jahn-Teller (JT) distortion and double exchange (DE) mechanism [7-8], the Mn-O bond length and Mn-O-Mn bond angle of MnO_6 had to be taken into consideration. Lattice distortion will alter the crystal structure of the system which then

indirectly disturb the magnetic as well as the conducting mechanism. Moreover, the microstructure features and surface morphology will also influence the electrical transport behavior as well [3, 9]. In this work, we report the experimental results concerning structure and microstructure of $LaMnO_3$ and $La_{0.67}Ba_{0.33}MnO_3$ system in bulk and thin films form respectively. A comparison on structure and microstructure among the fabricated samples were then shown.

EXPERIMENTAL DETAILS

Bulk $LaMnO_3$ (LMO) and $La_{0.67}Ba_{0.33}MnO_3$ (LBMO) were prepared via solid state reaction with stoichiometric amount of La_2O_3, $BaCO_3$, and $MnCO_3$ as starting powders. These high purity powders (99.9%) were wet milled in acetone and dried at 100 °C for 4 hours. Calcination at 900 °C for 12 hours was introduced after the dried powders were ground. Subsequently, these powders were reground and sieved with 38 μm sieve size before press into pellets. The pelletized powders were sintered at 1300 °C for 24 hours.

Thin films sample were fabricated using Pulsed Laser Deposition (PLD) technique with synthesized LMO and LBMO as target. The deposition was carried out using Nd-YAG laser of wavelength 1064nm with energy of 1.5 J/pulse at a pulse repetition rate of 10 pps. Before deposition, the substrate which located parallel 4 cm from the target was stabilized at 400°C in the oxygen pressured of 7×10^{-2} mbar. During deposition, the power density of the focused laser beam on the rotating target was about 4.7×10^5 W/cm^2 and the deposition time was half an hour. After deposition, the film was cooled down slowly and trapped in surrounding of 2 mbar oxygen before post annealed in air at 700 °C for 4 hours. Under these circumstances, LMO was growth on amorphous corning glass (1737), amorphous fused silica (JGS1) and single crystal MgO oriented (100) so-called LMO-CG, LMO-FS and LMO-M respectively. For LBMO thin film grew on corning glass, fused silica and MgO (100), were named as LBMO-CG, LBMO-FS and LBMO-M respectively.

In structure characterization, X-ray diffraction (XRD, Phillips PW 3040/60 Xpert Pro) technique with radiation of CuKα was performed in continuous scan mode with step size of 0.033° within the range of 20-80°. For bulk samples, Gonio (2θ-θ) scan was used while 2θ scan with gracing angle of 2° for thin films. The XRD data collected were analyzed by Rietveld refinement technique with X'Pert HighsScore Plus program. For microstructure viewing, Variable Pressure Scanning Electron Microscope (VPSEM, LEO 1455 VPSEM) was used to view bulk sample and higher magnification needed for thin film samples which can be fulfilled by Field Emission Scanning Electron Microscope (FESEM, Zeiss SUPRATM 55VP).

Solid State Science and Technology, Vol. 19, No2 (2011) 249-258
ISSN 0128-7389

RESULTS AND DISCUSSION

The X-ray diffraction spectrums of the LMO in bulk and thin film are shown in Figure 1. All samples revealed single phase which matched the ICSD standard (ICSD Code: 98-003-9308). From the inset in Figure 1 which taken from the most intense peak (31.0°~34.5°) from all samples, the spectrums contributed by thin film sample show broader peaks as compared to bulk sample. Different pattern of XRD spectrum was observed between bulk and thin film LMO, this probably due to dissimilar crystal system in both samples.

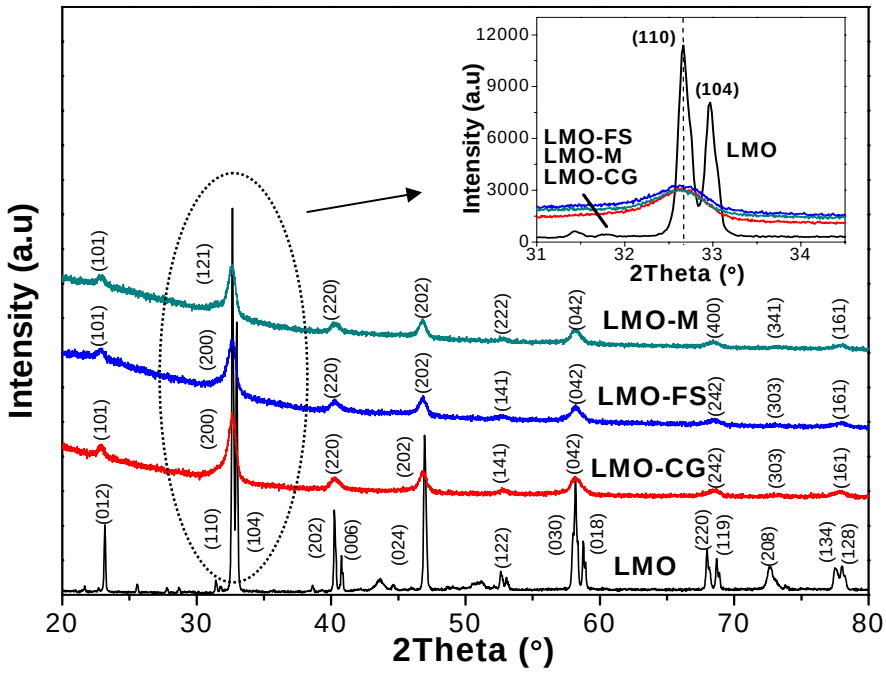

Figure 1: XRD spectrums of LMO in bulk and thin films

The lattice parameters of all LMO samples obtained by refining the experimental data using Rietveld refinement technique are tabulated in Table 1. As observed in Table 1, the crystal system of LMO in bulk was trigonal and transformed to orthorhombic after converted to thin film. The structure transformation is probably due to elimination of defects resulted from lattice misfit by some bond stretching or atoms relocation in film during film deposition through layer-by-layer and/or island growth mechanism [10]. On the other hand, a significant change in volume of unit cell was observed between bulk and thin films. We calculated that volume of unit cell of LMO was 409 $Å^3$ in bulk and around 232 $Å^3$ for thin films. The unit cell of LMO thin films are denser than bulk LMO since volume is inversely proportional to density.

Table 1: Refined crystallography data of LMO, LMO-CG, LMO-FS and LMO-M

Sample code	LMO	LMO-CG	LMO-FS	LMO-M
Crystal System	Trigonal	Orthorhombic	Orthorhombic	Orthorhombic
Space Group	*R-3c*	*Pnma*	*Pnma*	*Pnma*
Lattice parameter				
a (Å)	5.5320 (2)	5.4510 (1)	5.4520 (2)	5.4560 (2)
b (Å)	5.5320 (2)	7.7230 (2)	7.7250 (3)	7.7330 (3)
c (Å)	13.3664 (7)	5.5190 (1)	5.5210 (2)	5.5150 (2)
Volume of cell ($Å^3$)	409.0523	232.3393	232.5263	232.6847
Density (g/cm^3)	6.8007	6.9059	6.9080	6.9027
Crys. size, D (nm)	151.6	14.2	21.8	15.5
Lattice strain (%)	0.136	0.934	0.628	0.788
Mn-O(1)-Mn (°)	165.8 (3)	161.3 (3)	161.0 (4)	153.3 (2)
Mn-O(2)-Mn (°)		167.5 (4)	166.4 (3)	170.2 (4)
Mn-O(1) (Å)	1.9620 × 6	1.853 × 2	1.812 × 2	1.992 × 2
		2.081 × 2	2.121 × 2	1.995 × 2
Mn-O(2) (Å)		1.942 × 2	1.945 × 2	1.940 × 2
R_{exp} (%)	4.5611	3.0461	2.7234	2.9078
R_{pr} (%)	8.1053	3.1288	2.6529	2.7454
R_{wpr} (%)	12.7308	4.0509	3.3813	3.5202
Goodness of fit	8.4306	1.7685	1.5415	1.4656

The crystallite size were calculated using Scherrer's formula, $S = K\lambda/\beta\text{Cos}\theta$, where S is average particle size in nm, K is a constant (shape factor; 0.89), θ is Bragg's angle from the most intense peak, λ is CuKα wavelength and β is the corrected full-width half-maxima (FWHM) of the XRD peaks of all sample [11]. The lattice strain was calculated using X'Pert HighScore Plus program. The lattice strain was 0.136 %, 0.934%, 0.628% and 0.788% for LMO, LMO-CG, LMO-FS and LMO-M respectively. From the calculated lattice strains, thin film LMO experienced higher lattice strain compared to bulk. A variation was observed where higher lattice strain (LMO-CG) display smaller crystallite size (14.2nm). In thin film sample, unavoidable strain from lattice misfit between film and substrate are expected [6, 12-13]. This might cause LMO to grow in stretched condition and hence smaller crystallite size was observed. Conversely, structure and grain growth in bulk are freely, random and disorder. Therefore, less lattice strain was observed in bulk LMO with bigger crystallite size and less dense structure.

In bulk LMO, Mn-O-Mn bond angle and Mn-O bond length observed in MnO_6 octahedron are constant and symmetry. Upon converted to thin film, crystal structure transformation occur resulting bond angle and bond length turn out to be uneven (asymmetry). Thus, dissimilar bond angle and bond length can be detected. This might

due to strain induced from lattice misfit resulted MnO_6 octahedron to be elongated or compressed. Beside that, bond angle and bond length of LMO-CG and LMO-FS are almost similar but slightly different as compared to LMO-M. These might due to the properties of substrate used where corning glass and fused silica are amorphous whereas MgO is single crystal.

From Figure 2, the SEM micrographs of bulk LMO shows grains with average grain sizes of 7-9 μm. For LMO-FS, LMO-CG and LMO-M films, melted-like grains were observed. The surface morphology are almost similar with average grain sizes of 40-60 nm in 100,000X magnification (inset of Figure 2). At the same time, thin film samples shows rounded piles of grains indicating island growth mode [3]. In fact, the microstructure formation initially is layer-by-layer growth. Due to lattice misfit between film and substrate, strain was created and lead to island like growth [10].

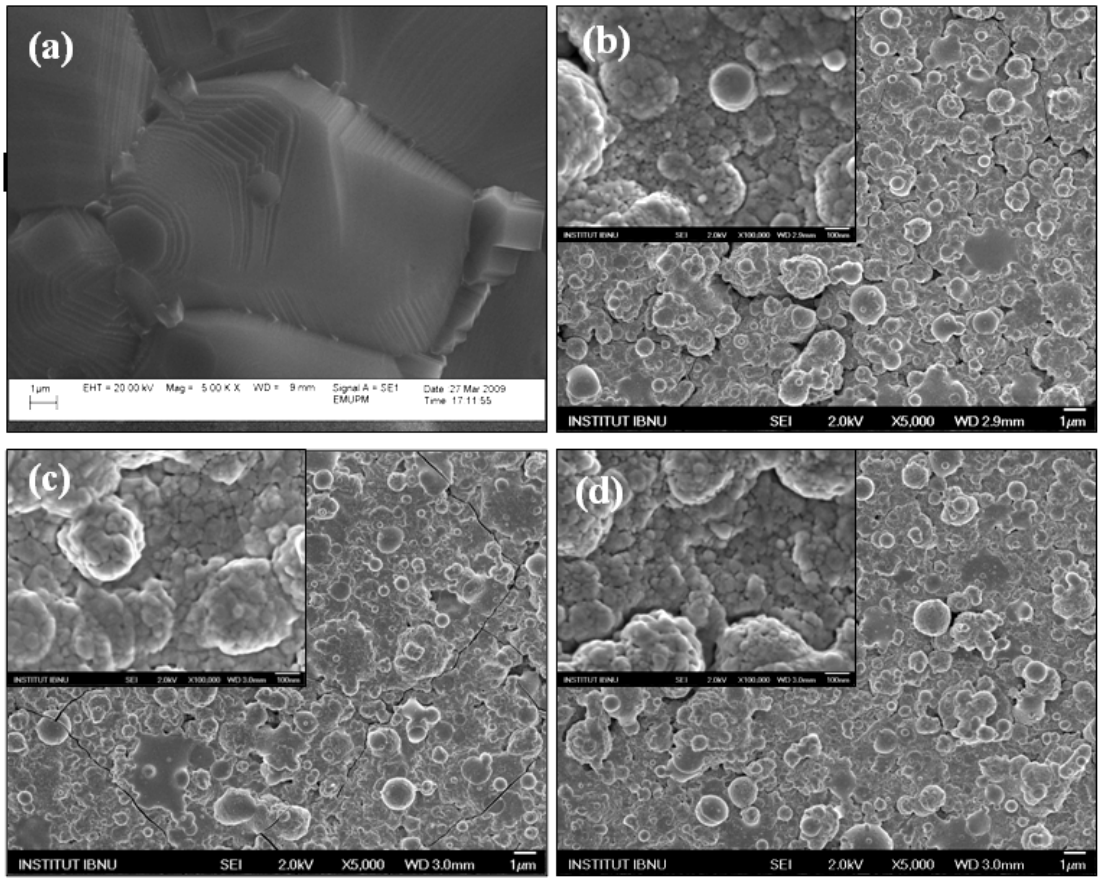

Figure 2: SEM micrographs of (a) LMO, (b) LMO-CG, (c) LMO-FS and (d) LMO-M with magnification of 5,000X (the inset shows 100,000X)

XRD patterns of LBMO samples as illustrated in Figure 3 are single phase which matched the ICSD standard (ICSD Code: 98-005-8163). The XRD data of all LBMO

were refined using Rietveld refinement technique and tabulated in Table 2. Orthorhombic crystal system was observed in all LBMO samples. The inset in Figure 3 showed the most intense peak (31.0°~34.0°) of all LBMO samples. Bulk LBMO shown a sharp and higher intense peak (FWHM smaller) while LBMO thin film sample gave broaden peak. This point out that crystallite size of bulk LBMO is larger as compared to LBMO thin film and agreed with the calculated value using Scherrer's equation [11] (refer Table 2).

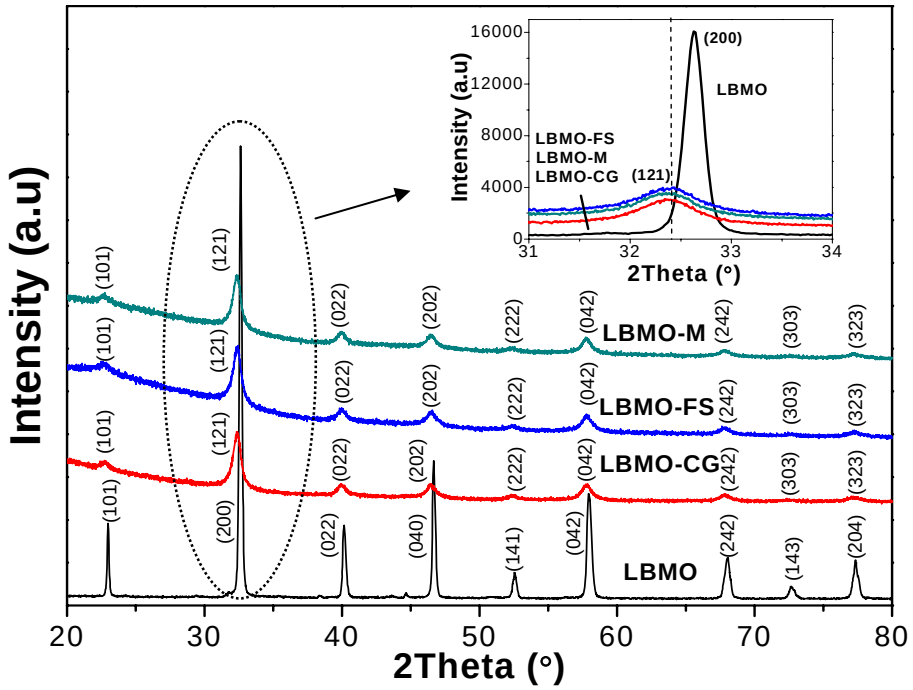

Figure 3: XRD patterns of LBMO in bulk and thin films

In additional, main peaks contributed by LBMO thin film were found at lower 2Theta as compared to bulk LBMO. Since *d*-spacing, *d* is inversely proportional to Sinθ (Bragg's law: λ=2*d*Sinθ), shifting of these peaks to lower 2Theta shows increment of *d*-spacing. At the same time, lattice parameter *c* of LBMO films (LBMO-CG, LBMO-FS and LBMO-M) is larger compared to bulk LBMO. We believe that the increment of lattice parameter *c* is related to the increase of *d*-spacing since lattice parameter *c* represent height of unit cell in *c*-axis while *d*-spacing is spacing between atomic planes. Therefore, it is reasonable that increase of *d*-spacing consequently increase the lattice parameter *c*. Nevertheless, deformation of unit cell was observed between bulk and thin film LBMO. Lattice parameter *a* and *b* of LBMO thin film are smaller as compared to bulk LBMO while lattice parameter *c* of LBMO thin film is larger than bulk LBMO (refer Table 2). This emphasis a sign of positive misfit [6] to LBMO thin film (the unit cell compressed along *a*-*b* axis and elongate along *c*-axis) after converted from bulk LBMO. In fact, when a different material is deposited onto substrate, misfit between films and substrate could occur [13].

Table 2: Refined crystallography data of bulk LBMO, LBMO-CG, LBMO-FS and LBMO-M

Sample code	LBMO	LBMO-CG	LBMO-FS	LBMO-M
Crystal System	Orthorhombic	Orthorhombic	Orthorhombic	Orthorhombic
Space Group	*Pnma*	*Pnma*	*Pnma*	*Pnma*
Lattice parameter				
a (Å)	5.5214 (2)	5.5200 (1)	5.5160 (2)	5.5180 (1)
b (Å)	7.8156 (3)	7.7860 (2)	7.7860 (2)	7.7870 (2)
c (Å)	5.5466 (2)	5.5610 (3)	5.5620 (4)	5.5610 (3)
Volume of cell ($Å^3$)	239.3520	239.0047	238.8744	238.9488
Density (g/cm^3)	6.6957	6.7048	6.7099	6.7070
Crys. size, D (nm)	63.0	14.0	13.5	15.2
Lattice strain (%)	0.258	0.954	0.986	0.880
Mn-O(1)-Mn (°)	160.4 (2)	163.2 (6)	162.9 (3)	162.2 (2)
Mn-O(2)-Mn (°)	163.5 (3)	161.4 (4)	159.9 (5)	160.4 (6)
Mn-O(1) (Å)	1.793×2 2.177×2	1.893×2 2.068×2	1.892×2 2.069×2	1.861×2 2.103×2
Mn-O(2) (Å)	1.974×2	1.972×2	1.977×2	1.976×2
R_{exp} (%)	4.7462	3.2006	2.5797	2.7978
R_{pr} (%)	6.9667	2.7699	2.2088	2.4098
R_{wpr} (%)	9.4410	3.5076	2.8464	3.0645
Goodness of fit	3.9568	1.2011	1.2174	1.1997

Conversely, the calculated lattice strain using X'Pert HighScore Plus program gives bulk LBMO the lowest value (0.258%) compared to LBMO-FS (0.986%), LBMO-CG (0.954%) and LBMO-M (0.880%) respectively. These suggest that lattice misfit occur in LBMO thin film where large lattice strain was observed. In fact, bond stretching or atoms relocation often occur to eliminate defects created from lattice misfit. Therefore, larger lattice strain is expected in LBMO thin film. Consequently, lattice strain can enhance density of LBMO thin film with compression force caused by lattice misfit. From Table 2, larger lattice strains promote denser crystal system with smaller crystallite size.

On the other hand, slight change in Mn-O-Mn bond angle and Mn-O bond length was observed between strained thin film and bulk LBMO (MnO_6 octahedron). As observed, the changes of bond length take place in Mn-O(1) where longest or shortest bond length can be found in bulk LBMO. Once converted to LBMO thin film (strained), bond length and bond angle of both LBMO-CG and LBMO-FS are quite similar compared to LBMO-M. These probably due to the influences of substrate used which cause different type of lattice strain [6, 9].

Solid State Science and Technology, Vol. 19, No2 (2011) 249-258
ISSN 0128-7389

Figure 4 shows the SEM micrographs of LBMO samples. The average grain sizes of bulk LBMO are around 0.5-1.5 μm. However, no clear grain boundaries can be observed in LBMO thin films with magnification up to 100,000X (inset of Figure 4). Strong diffusion occurred where grains necked and form melted-like microstructure. Minor island growth mode was observed. In additional, nano-sized cracks were observed in thin film samples (refer Figure 4). A variation of crack size was observed and might relate to the coefficient of thermal expansion of substrate used. The crack size follow sequence of LBMO-FS > LBMO-CG > LBMO-M with coefficient of thermal expansion of fused silica (5.50×10^{-7} °C^{-1}) [14] > corning glass (3.76×10^{-6} °C^{-1}) [15] > MgO (1.28×10^{-5} °C^{-1}) [16] respectively. We believe that there are dissimilarity in expansion or shrinkage between film and substrate during heating or cooling treatment (thermal stress) [13]. In additional, LBMO-FS has obvious and larger cracks as compared other which probably due to smaller coefficient of thermal expansion and could invoke greater thermal stress. In contrast, no obvious cracks can be detected in LMO thin film samples. The barium doped in LMO (LBMO) might change the coefficient of thermal expansion for LMO.

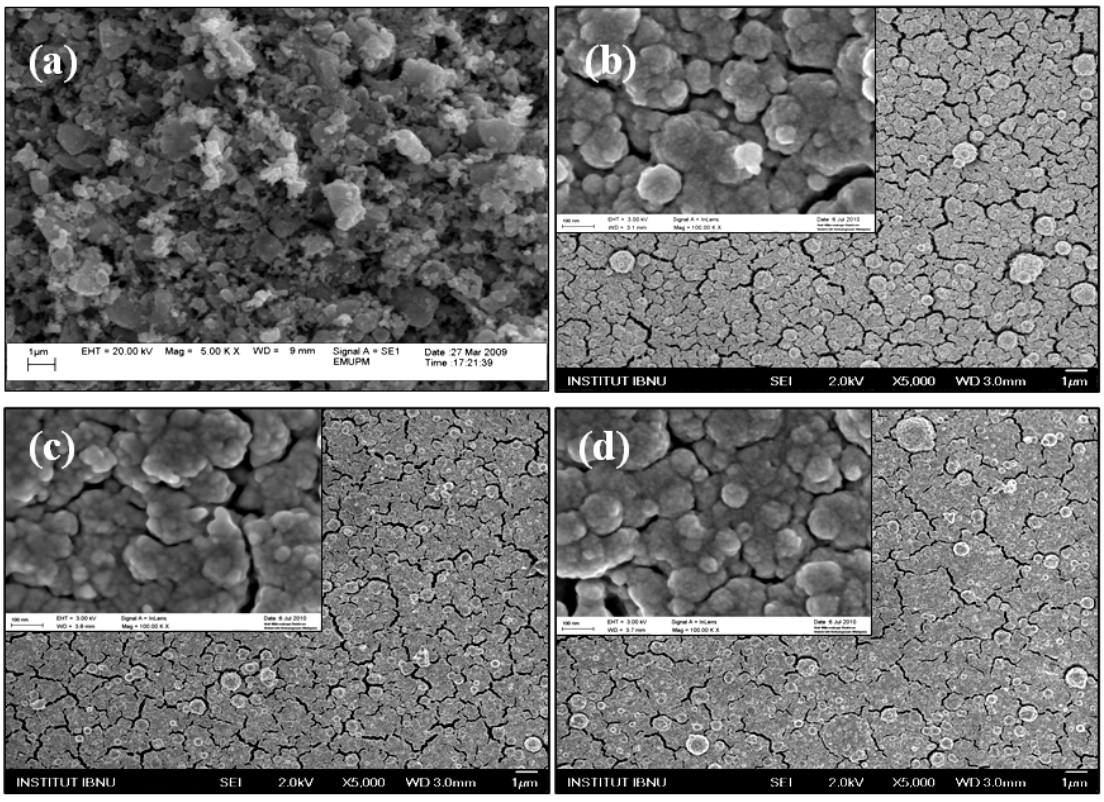

Figure 4: SEM micrographs of (a) bulk LBMO, (b) LBMO-CG, (c) LBMO-FS and (d) LBMO-M with magnification of 5,000X (the inset shows 100,000X)

Solid State Science and Technology, Vol. 19, No2 (2011) 249-258
ISSN 0128-7389

CONCLUSION

Lattice strains are responsible for crystal structure growth where higher lattice strain was observed in thin film due to lattice misfit. Crystal structure transformation was observed on LMO when converted from bulk to thin film while LBMO shows positive misfit. Melted-like (nano-sized) grains with island growth mode were observed in all thin film samples. Nano-sized cracks were observed in thin film LBMO due to different in coefficient of thermal expansion of substrate used. Smaller coefficient of thermal expansion gives more and large crack sizes.

ACKNOWLEDGEMENT

The Ministry of Higher Education Malaysia (MOHE) is gratefully acknowledged for the grant under Fundamental Research Grant Scheme (FRGS) vote: 5523756: Effect of Nanoparticles on low-field magnetoresistance of $Ln_{1-x}A_xMnO_3$ ceramic, Research University Grant Scheme (RUGS) vote 91849: Low-Field Magnetoresistance effect in polycrystalline $Ln_{1-x}A_xMnO_3$ ceramic thin films and Ministry of Science, Technology and Innovation Malaysia (MOSTI) for National Science Fellowship (NSF) scholarship.

REFERENCES

[1] R. von Helmolt, J. Wecker, B. Holzapfel, L. Schultz and K. Samwer, *Phys. Rev. Lett.* **71** (1993) 2331-2333
[2] S. Jin, M. McCormack, T. H. Tiefel and R. Ramesh, *J. Appl. Phys.* **76** (1994) 6929-6933
[3] N.-C. Yeh, C.-C. Fu, and J. Y. T. Wei, R. P. Vasquez, J. Huynh and S. M. Maurer G. Beach and D. A. Beam *J. Appl. Phys.* **81** (1997) 5499-5501
[4] X. Guo, S. Dai, Y. Zhou, G. Yang, and Z. Chen, *Appl. Phys. Lett.* **75** (1999) 3378-3380
[5] A. P. Ramirez. *J. Phys.: Condens. Matter.* **9** (1997) 8171-8199
[6] G. Van Tendeloo, O. I. Lebedev, M. Hervieu and B. Raveau. *Rep. Prog. Phys.* **67** (2004) 1315-1365
[7] P. G. De Gennest *Phys. Rev.* **118** (1960) 141-154
[8] C. Zener *Phys. Rev.* **81** (1951) 403-405
[9] V. G. Prokhorov, V. S. Flis, and G. G. Kaminsky and Y. P. Lee, *Low Temp. Phys.* **30** (2004) 463-468
[10] L. W. Martin, Y.-H. Chu and R. Ramesh, *Mat. Sci. Eng. R* **68** (2010) 89-133
[11] D.C. Krishna and P. Venugopal Reddy, *J. Alloy. Compd*. **479** (2009) 661-669
[12] K. A. Thomas, P. S. I. P. N. de Silva, L. F. Cohen, A. Hossain, M. Rajeswari, T. Venkatesan, R. Hiskes and J. L. MacManus-Driscoll *J. Appl. Phys.* **84** (1998) 3939-3947
[13] M. Ohring Materials Science of Thin Films (Second Edition): Deposition and Structure, (Elsevier Inc. Sciencedirect, 2002)
[14] New Rise Optics, llc, http://www.newrise-llc.com/fused-silica.html (accessed 27 Sept 2010)

[15] Praezisions Glas & Optik GmbH,
http://www.pgo-online.com/intl/katalog/1737.html (accessed 27 Sept 2010)
[16] MTI Corporation
http://www.mtixtl.com/mgo100substrate10x10x05mm1spqtydiscounted.aspx
(accessed 27 Sept 2010)